nature astronomy

Supplementary information

https://doi.org/10.1038/s41550-025-02651-2

# A million-solar-mass object detected at a cosmological distance using gravitational imaging

In the format provided by the authors and unedited

# Supplementary Figures

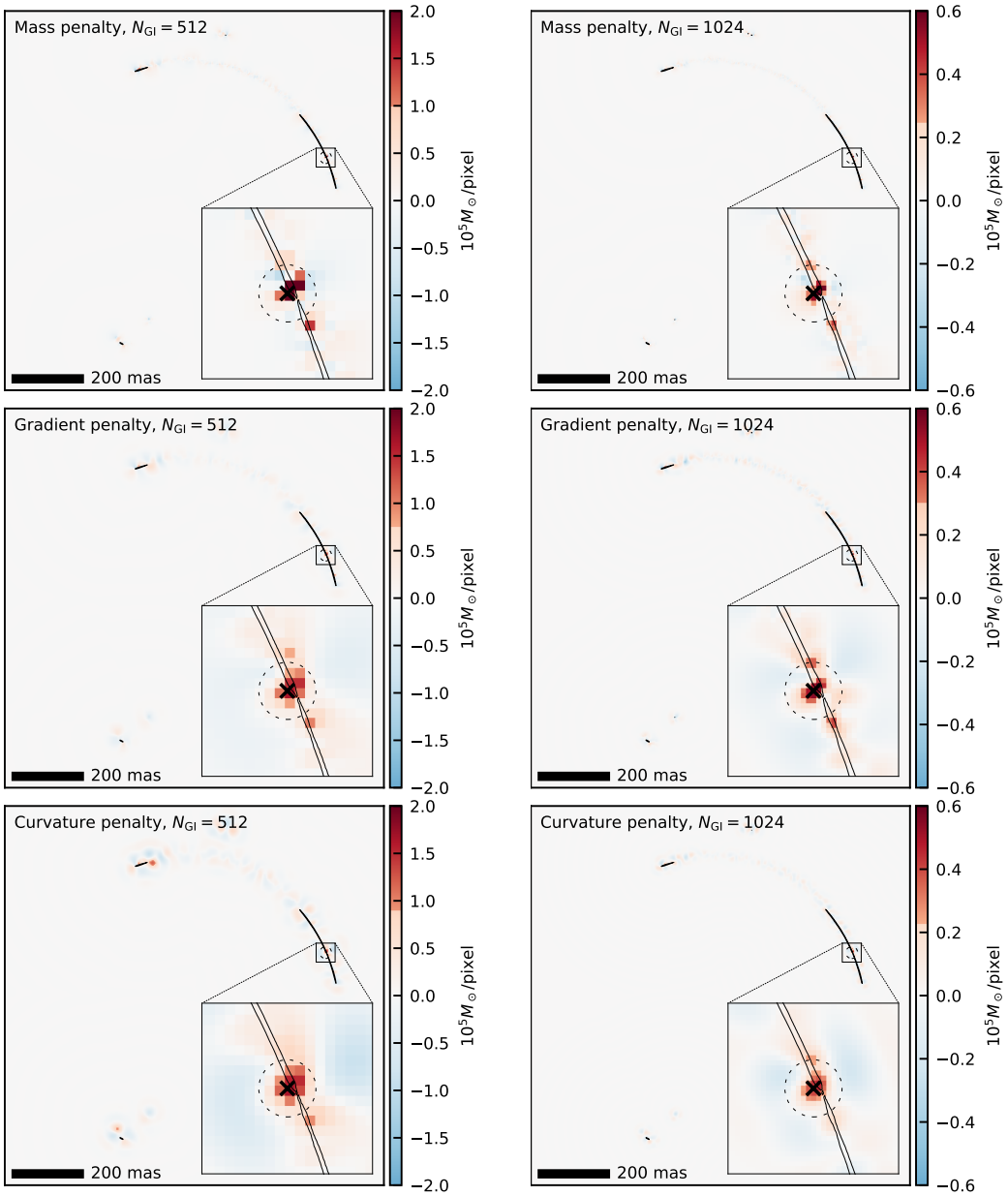


**Supplementary Figure 1** Non-parametric gravitational imaging (GI) corrections to the lensing convergence (expressed in units of lens-plane surface mass density), for six different combinations of regularization type and grid resolution $N_{\rm GI}$. The discontinuities in the intensities of the colour scales indicate the $3\sigma_{\rm GI}$ thresholds used to identify features of interest in the convergence corrections. In all six GI runs, we recover compact, positive convergence features in the same location along the bright arc. These positions are consistent with the independent parametric modeling results for detection $\mathcal{V}$, whose location is shown by the black X's. The dashed black circles in the inset panels have a radius of 80 pc. The lensed images are indicated by the black contours.

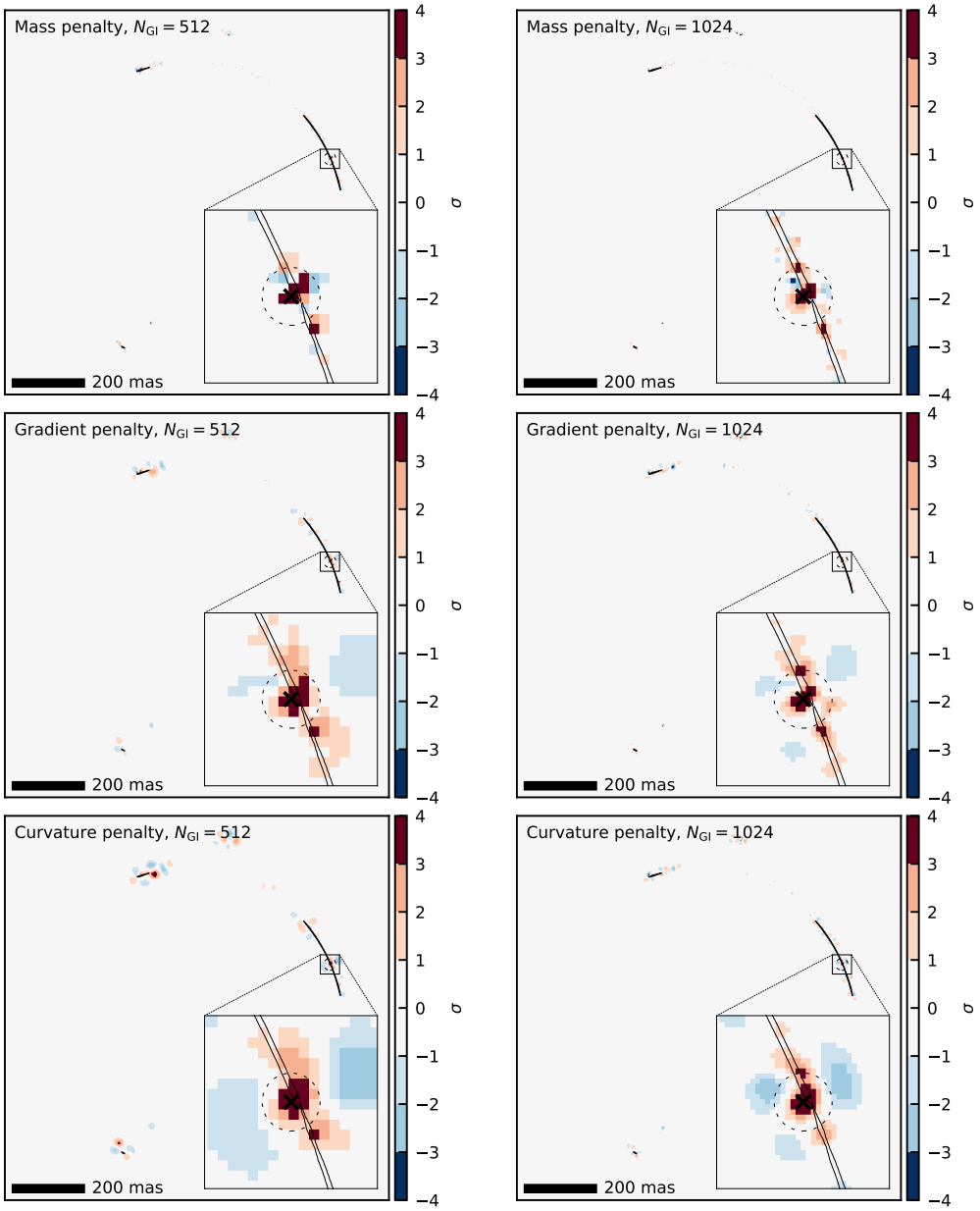


**Supplementary Figure 2** Significance map for gravitational imaging (GI) corrections to the lensing convergence, expressed in units of $\sigma_{\rm GI}$. While features above the $3\sigma_{\rm GI}$ threshold appear at various locations in some of the runs, only the feature associated with detection $\mathcal{V}$ (black X's) is robust and consistent across all six different combinations of regularization type and grid resolution $N_{\rm GI}$. See Supplemental Figure 1 for GI maps in units of surface mass density.

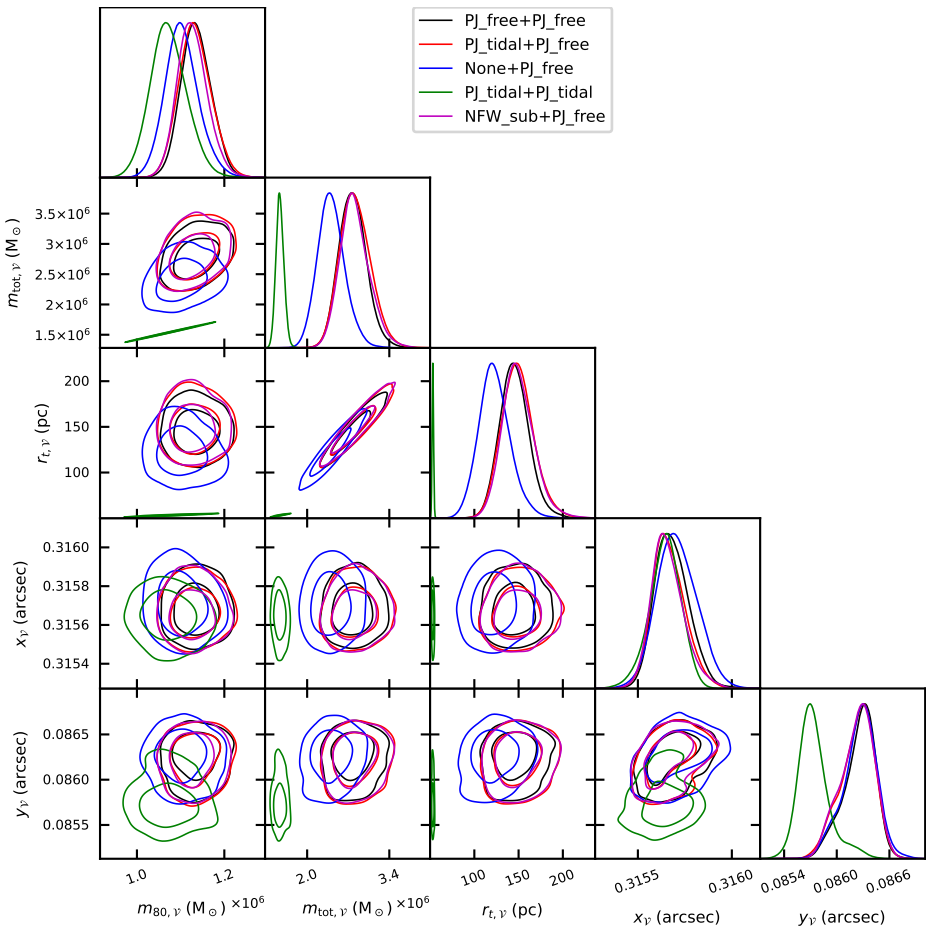


**Supplementary Figure 3** Parametric modeling results for detection $\mathcal{V}$. $m_{80,\mathcal{V}}$ is the cylindrical mass contained within a radius of 80 pc, where the data are most sensitive to the enclosed mass (see the main text). When the mass of $\mathcal{V}$ is expressed as $m_{80,\mathcal{V}}$ rather than $m_{\mathrm{tot},\mathcal{V}}$, the properties of $\mathcal{V}$ are consistent across all models. This indicates that the inferred properties of detection $\mathcal{V}$ are robust to the model parameterization for detection $\mathcal{A}$. $m_{80,\mathcal{V}}$ is derived from $m_{\mathrm{tot},\mathcal{V}}$ and $r_{t,\mathcal{V}}$, and is not a free parameter. Likewise, the tidal radius $r_{t,\mathcal{V}}$ of $\mathcal{V}$ = `PJ_tidal` is derived from the lens and perturber masses and positions.

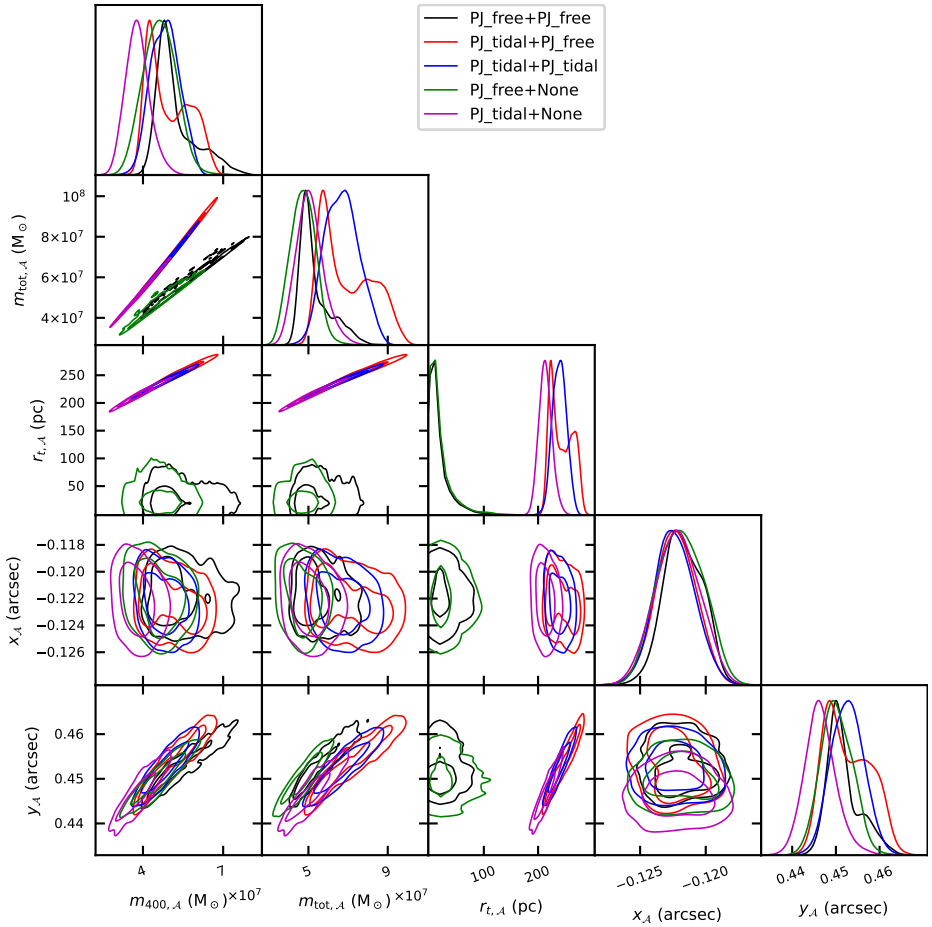


**Supplementary Figure 4** Parametric modeling results for detection $\mathcal{A}$, for runs where $\mathcal{A}$ is modeled as pseudo-Jaffe (PJ) subhalo profile. $m_{400,\mathcal{A}}$ is the cylindrical mass contained within a radius of 400 pc, which is the transverse distance between the position of $\mathcal{A}$'s center and the nearest lensed radio emission. Hence, we expect only $m_{400,\mathcal{A}}$ rather than $m_{\mathrm{tot},\mathcal{A}}$ to be robustly constrained by the data, and find that it is consistent between all runs. Meanwhile $r_{t,\mathcal{A}}$ is unconstrained and always less than 400 pc, which simply reflects the tidal radius relation or the log-uniform prior. $m_{400,\mathcal{A}}$ is roughly consistent with the findings of Despali et al. (see main text), who infer $m_{400,\mathcal{A}} = (7.7 \pm 0.1) \times 10^7$ from a Keck AO observation of JVAS B1938+666. $m_{400,\mathcal{A}}$ is derived from $m_{\mathrm{tot},\mathcal{A}}$ and $r_{t,\mathcal{A}}$, and is not a free parameter. Likewise, the tidal radius $r_{t,\mathcal{A}}$ of $\mathcal{A}$ = `PJ_tidal` is derived from the lens and perturber masses and positions.

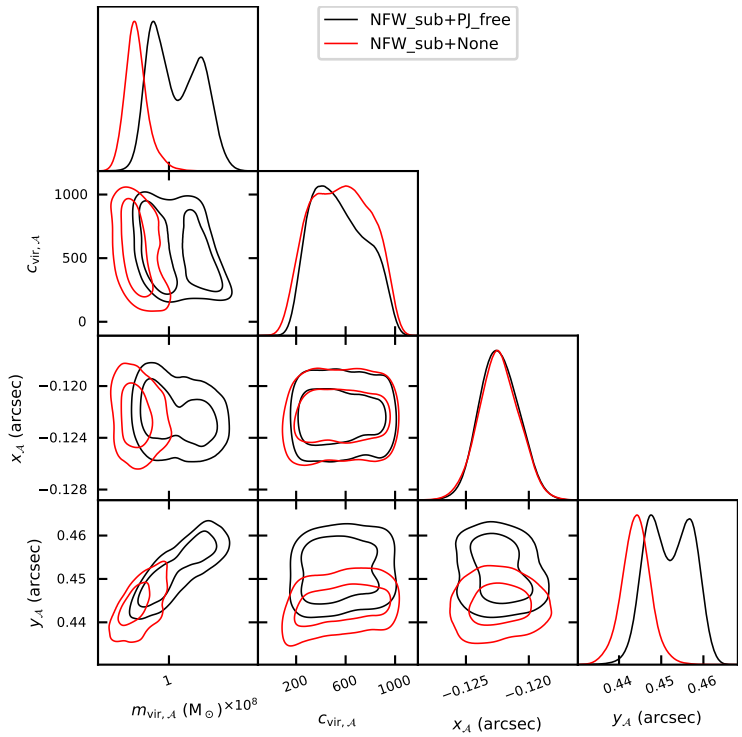


**Supplementary Figure 5** Parametric modeling results for detection $\mathcal{A}$, for runs where $\mathcal{A}$ is modeled as an NFW profile fixed to the lens redshift of $z = 0.881$. The virial concentration $c_{\mathrm{vir},\mathcal{A}}$ is unconstrained, reflecting the fact that the nearest lensed radio emission lies 400 pc from the center of $\mathcal{A}$, and therefore lacks constraining power over the density profile of $\mathcal{A}$ within 400 pc. Interestingly, the inclusion of detection $\mathcal{V}$ in the lens model introduces a second mode in the posterior distribution of $\mathcal{A}$'s parameters. This sensitivity to the global lens mass distribution, in contrast with $\mathcal{V}$, is due to the fact that $\mathcal{A}$ does not lie directly on top of lensed radio emission as $\mathcal{V}$ does.

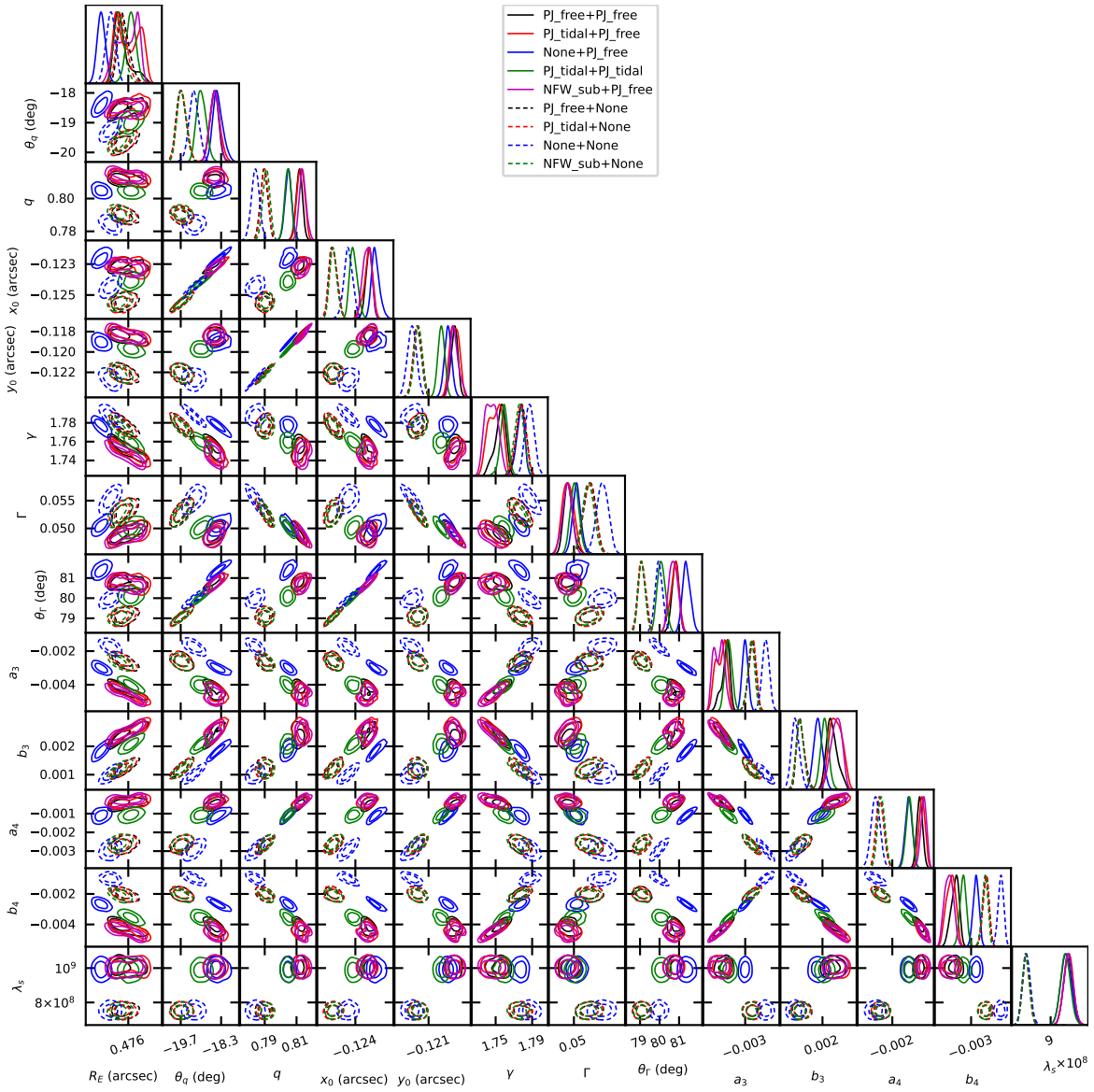


**Supplementary Figure 6** Posterior distributions of macro-model parameters for all parametric models. Models including $\mathcal{V}$ are shown in solid contours, while models without $\mathcal{V}$ are shown in dashed contours. Inferred properties of the main lens profile are mostly sensitive to the presence or absence of $\mathcal{V}$. In particular, the shape of the main lens (the axis ratio $q$ and multipole coefficients $a_3$, $b_3$, $a_4$, $b_4$) changes depending on whether or not $\mathcal{V}$ is present. Most notable, however, is the consistent increase in the preferred value of the source regularization hyper-parameter $\lambda_{\boldsymbol{s}}$ when $\mathcal{V}$ is included in the model. This reflects the fact that the source reconstruction is better-focused, and hence smoother, than in the case without $\mathcal{V}$; see Figure 2 of the main text.